

**Wide-angle, azimuthal angle-independent and dual-band infrared
metamaterial absorber based on asymmetric structure**

A DISSERTATION

SUBMITTED IN FULFILLMENT OF THE REQUIREMENTS

FOR THE AWARD OF THE DEGREE OF

MASTER OF SCIENCE

IN

PHYSICS

Submitted by:

SUSHANT PANDIT

2K23/MSCPHY/48

Under the supervision of

DR. KAMAL KISHOR

(Assistant Professor, Department of Applied Physics, DTU)



DEPARTMENT OF APPLIED PHYSICS

DELHI TECHNOLOGICAL UNIVERSITY

(Formerly Delhi College of Engineering)

Bawana Road, Delhi – 110042

JUNE, 2025

DELHI TECHNOLOGICAL UNIVERSITY

(Formerly Delhi College of Engineering)

Bawana Road, Delhi – 110042

CANDIDATE'S DECLARATION

I hereby certify that the work which is presented in the Dissertation-II titled “Wide-angle, azimuthal angle-independent and dual-band infrared metamaterial absorber based on asymmetric structure” in fulfilment of the requirement for the award of the Master of Science in Physics and submitted to the Department of Applied Physics, Delhi Technological University, Delhi is an authentic record of my own, carried out during a period from January 2025 to May 2025, under the supervision of Dr. Kamal Kishor.

The matter presented in this report/thesis has not been submitted by me for the award of any other degree of this or any other Institute/University.

Title of the Paper: Wide-angle, azimuthal angle-independent and dual-band infrared metamaterial absorber based on asymmetric structure

Author names: Sushant Pandit, Ankit, Kamal Kishor

Name of Conference/Journal:

Conference Dates with venue (if applicable):

Have you registered for the conference (Yes/No)? No

Status of paper (Accepted/Published/Communicated):

Date of paper communication:

Date of paper acceptance:

Date of paper publication:



SUSHANT PANDIT

23/MSCPHY/48

SUPERVISOR CERTIFICATE

To the best of my knowledge, the above work has not been submitted in part or full for any Degree or Diploma to this University or elsewhere.

Place: Delhi


Dr. KAMAL KISHOR

Date: 9th June, 2025

ABSTRACT

A wide-angle, azimuthal angle-independent and dual-band metamaterial absorber in the mid-infrared region is proposed which is made of copper and SiC. SiC dielectric is sandwiched between a copper layer at the bottom and a design made of copper on the top. For the proposed metamaterial absorber, simulation results show absorption peaks at two different wavelengths. It is due to magnetic polariton modes produced at those two wavelengths of mid-infrared region. Moreover, the simulation results also show a good impedance matching the metamaterial absorber and the air (or vacuum). Good absorption by the proposed structure has been observed for incident angles θ spanning from 0° to 80° at azimuthal incident angle $\phi = 0^\circ$ and 90° for both TE and TM incidences. In addition, the proposed structure also shows good absorption for azimuthal incident angles ϕ spanning from 0° to 180° at $\theta = 45^\circ$ because perpendicular magnetic polariton modes were excited within the proposed asymmetric structure. Therefore, the proposed structure can be used for applications in infrared spectroscopy and imaging.

ACKNOWLEDGEMENT

I would like to thank my supervisors Dr. Kamal Kishor and Dr. Ankit for their guidance in the dissertation project. In addition, I would like to thank the Department of Applied Physics, Delhi Technological University.

Place: Delhi

Date: 9th June, 2025



SUSHANT PANDIT

CONTENTS

Candidate's declaration.....	i
Supervisor certificate.....	ii
Abstract.....	iii
Acknowledgement.....	iv
Contents.....	v-vi
List of Tables.....	vii
List of Figures.....	viii-ix
1. Introduction to metamaterials.....	1-3
1.1. Introduction	
1.2. History of metamaterials	
2. Types of metamaterials.....	4-5
2.1. Electromagnetic metamaterials	
2.2. Elastic metamaterials	
2.3. Acoustic metamaterials	
2.4. Thermal metamaterials	
2.5. Nonlinear metamaterials	
3. Applications of metamaterials.....	6-7
3.1. Metamaterial antennas	
3.2. Metamaterial absorber	
3.3. Superlens	
3.4. Cloaking device	
3.5. Radar cross-section (RCS) reducing metamaterials	
3.6. Seismic metamaterials	
3.7. Acoustic metamaterials	

4. Design and method.....	8-10
5. Results and discussion.....	11-23
6. Conclusion.....	24
7. References.....	25-28
Appendix 1: Plagiarism report.....	29-32

LIST OF TABLES

Table 4.1 Unit cell dimension

Table 5.1 Dual-band absorption at different incident angles

Table 5.2 Range of θ in which absorptivity is satisfactory

Table 5.3 Range of ϕ in which absorptivity is satisfactory

LIST OF FIGURES

Fig. 4.1. (a) Top view, (b) side view and (c) TE wave incident on the structure from x-z plane with an incident angle of θ with z-direction and azimuthal incident angle $\phi = 0^\circ$ of the proposed unit cell of the metamaterial absorber

Fig. 5.1. (a) Absorption response of the designed metamaterial absorber under normal incidence ($\theta = 0^\circ$), with the electric field vibrations of the mid-infrared wave along the y-direction (E_y) and x-direction (E_x), (b) Real and imaginary components of the effective impedance for y-polarized electric field, and (c) Real and imaginary components of the effective impedance for x-polarized electric field

Fig. 5.2. Z-component of electric field distribution at the resonant wavelengths of $5.62\ \mu\text{m}$ and $7.80\ \mu\text{m}$ under normal incidence with electric field vibrations along the y-direction: (a) on the top copper layer at $5.62\ \mu\text{m}$, (b) on the bottom copper layer at $5.62\ \mu\text{m}$, (c) on the top copper layer at $7.80\ \mu\text{m}$, and (d) on the bottom copper layer at $7.80\ \mu\text{m}$

Fig. 5.3. Z-component of the electric field distribution under normal incidence with the electric field polarized along the x-direction: (a) on the top copper structure at the resonant wavelength of $5.60\ \mu\text{m}$, (b) on the bottom copper layer at $5.60\ \mu\text{m}$, (c) on the top copper structure at $8.05\ \mu\text{m}$, and (d) on the bottom copper layer at $8.05\ \mu\text{m}$.

Fig. 5.4. (a) Absorption spectra of the proposed metamaterial absorber under TE and TM polarized incidence at an oblique angle ($\theta = 45^\circ$, $\phi = 0^\circ$); (b) and (c) show the corresponding real and imaginary parts of the effective impedance for TE and TM polarizations, respectively.

Fig. 5.5. Z-component of the electric field distribution for TE-polarized incidence at an oblique angle ($\theta = 45^\circ$, $\phi = 0^\circ$): (a) on the top copper structure and (b) on the bottom copper layer at the resonant wavelength of $5.60\ \mu\text{m}$; (c) on the top copper structure and (d) on the bottom copper layer at the resonant wavelength of $7.82\ \mu\text{m}$.

Fig. 5.6. Z-component of the electric field distribution for TM-polarized incidence at an oblique angle ($\theta = 45^\circ$, $\phi = 0^\circ$): (a) on the top copper structure and (b) on the bottom copper layer at the resonant wavelength of $5.82\ \mu\text{m}$; (c) on the top copper structure and (d) on the bottom copper layer at the resonant wavelength of $8.00\ \mu\text{m}$.

Fig. 5.7. (a) Absorption spectra of the proposed metamaterial absorber under TE and TM polarized incidence at an oblique angle ($\theta = 45^\circ$, $\phi = 90^\circ$); (b) and (c) show the corresponding

real and imaginary components of the effective impedance for TE and TM polarizations, respectively.

Fig. 5.8. Z-component of the electric field distribution for TE-polarized incidence at an oblique angle ($\theta = 45^\circ$, $\phi = 90^\circ$): (a) on the top copper structure and (b) on the bottom copper layer at the resonant wavelength of $5.60 \mu\text{m}$; (c) on the top copper structure and (d) on the bottom copper layer at the resonant wavelength of $8.02 \mu\text{m}$.

Fig. 5.9. Z-component of the electric field distribution for TM-polarized incidence at an oblique angle ($\theta = 45^\circ$, $\phi = 90^\circ$): (a) on the top copper structure and (b) on the bottom copper layer at the resonant wavelength of $5.75 \mu\text{m}$; (c) on the top copper structure and (d) on the bottom copper layer at the resonant wavelength of $7.78 \mu\text{m}$.

Fig. 5.10. Absorption spectra of the proposed metamaterial absorber as the incident angle (θ) varies from 0° to 80° at $\phi = 0^\circ$: (a) for TE-polarized incidence, (b) corresponding colormap representation for TE incidence, (c) for TM-polarized incidence, and (d) corresponding colormap representation for TM incidence. Absorption intensity is illustrated using the colormap scale

Fig. 5.11. Absorption spectra of the proposed metamaterial absorber as the incident angle (θ) varies from 0° to 80° at $\phi = 90^\circ$: (a) for TE incidence, (b) corresponding colormap representation for TE incidence, (c) for TM incidence, and (d) corresponding colormap representation for TM incidence. Absorption intensity is illustrated using the colormap scale

Fig. 5.12. Absorption spectra for TE-polarized incidence at $\theta = 45^\circ$ as the azimuthal angle (ϕ) varies: (a) from 0° to 90° , (b) corresponding colormap representation for $\phi = 0^\circ$ to 90° , (c) from 90° to 180° , and (d) corresponding colormap representation for $\phi = 90^\circ$ to 180° . Absorption intensity is represented by the colormap.

Fig. 5.13. Absorption spectra for TM-polarized incidence at $\theta = 45^\circ$ as the azimuthal angle (ϕ) varies: (a) from 0° to 90° , (b) corresponding colormap representation for $\phi = 0^\circ$ to 90° , (c) from 90° to 180° , and (d) corresponding colormap representation for $\phi = 90^\circ$ to 180° . Absorption intensity is represented by the colormap

1. INTRODUCTION TO METAMATERIALS

1.1 Introduction

Metamaterials are those materials which are engineered to have the property which is not typically found in nature. The unit cell of the structure of a metamaterial is made in such a way that its properties are due to its structure rather than the materials used. One thing is kept in mind while making the metamaterial is that the unit cells of the metamaterial must be smaller than the wavelength of the wave that they are required to manipulate. Metamaterials can be made to manipulate many types of waves such as electromagnetic waves, seismic waves, acoustic waves by either reflecting, absorbing, or bending waves. They have a large amount of applications such as absorbing electromagnetic radiation either in broadband wavelength range or narrowband, medical devices, sports equipment, optical filters, sensor detection, solar power management, lasers, lenses for high gain antennas, shielding structures from earthquakes. They can also be used in creating superlens which can tackle the diffraction limit and help us see very small particles with high resolution which is not possible with a conventional microscope. Even invisibility can be achieved with electromagnetic metamaterials if the structure of the unit cell is made in such a way it bends light around it. The scope in metamaterials is very high. More and more research is being done in this field.

In simple words, metamaterials are those electromagnetic materials which have periodic dimensions smaller than the wavelength and exhibit unique properties which are not found in natural materials [1]. They have uniquely engineered electric permittivity and magnetic permeability [2]. They can be used for applications such as tunable negative refraction [3,4], superlens [5], and optical cloaking [6]. In 2008, Landy et al. proposed the first perfect metamaterial absorber for the microwave band [7].

Extensive research has since been conducted to improve and tailor metamaterial designs across a broad range of frequencies. Metamaterials designed with tunable and broadband characteristics have been demonstrated using various configurations including split-ring resonators and near-zero index structures [8–11]. By using inherent loss, with the aid of suitable structure's design of metamaterial, perfect metamaterial absorbers are created for particular wavelengths which ranges from the microwave region of the electromagnetic spectrum [7,12–15] to the optical wavelength region [9,16,17], along with the infrared region [18,19] due to the improved sensitivity in biological and chemical sensing applications [20–22]. By using a cross-pattern metamaterial, Liu et al. had created a mid-infrared absorber for a single-band

[23]. However, single-band infrared absorbers face limitations in applications such as spectroscopy and imaging [24], which motivates the development of dual-band or multi-band infrared absorbers and emitters. Liu et al. further researched on an absorber which could absorb two bands by setting up a sub-unit sideways to the original unit cell having cross-pattern [19]. Chen et al. also researched on a perfect absorber which could absorb two bands by disturbing the symmetrical shape of the cross-patterned structure [25]; however, such structures which are asymmetric are typically sensitive to polarization angles for incident waves. Ankit et al. [26] demonstrated a far-infrared metamaterial perfect absorber with dual-band performance and sensing capability, employing a symmetric resonator geometry to achieve polarization insensitivity while maintaining high absorption. Dual-band perfect absorbers have also been developed using elliptical nano disks for near-infrared wavelengths [27], and electric-field-coupled resonators for far-infrared waves [28]. In general, a symmetric structure [23,29] is preferred to ensure polarization-independent absorption. Additionally, compound unit cells [19,27,30–33], or multi-layered configurations [13,34,35] are often required to realize dual-band or multi-band perfect absorption, which increases the complexity of fabrication.

1.2 History of metamaterials

Efforts to manipulate electromagnetic waves were started at the end of 19th century. In 1898, JC Bose researched substances with chiral properties which could be considered as metamaterials. In 1967, Victor Veselago first described theoretically about negative-index metamaterials and proved that such materials could transmit light. In 1995, John M. Guerra designed a transparent grating which had dimensions in sub-wavelength range i.e. dimensions smaller than the wavelength. In 1999, John Pendry demonstrated that if a C-shaped split ring is kept in such a way that the direction of its axis is along the propagation of the wave, we could achieve permeability which is less than zero ($\mu < 0$ i.e. negative permeability). And in 2000, he was also the first one to find a method to design a left-handed metamaterial. According to him, a metallic wire shows negative permittivity ($\epsilon < 0$) if it is aligned along the direction of propagation of a wave. In the same year, experimental demonstration of electromagnetic metamaterials was reported by David R. Smith et al. He and his team horizontally stacked, periodically, split-ring resonators and thin wire structures. As time passed, more and more research were conducted in the field of metamaterials. In 2006, an invisibility cloak for microwave region was realized which was not perfect but still it was a great achievement. Since

then, researchers took keen interest in developing invisibility cloak which could bend visible light and make an object invisible. By 2007, many groups conducted experiments related to negative refractive index.

2. TYPES OF METAMATERIALS

There are various types of metamaterials such as electromagnetic metamaterials, acoustic metamaterials, elastic metamaterials, thermal metamaterials, structural metamaterials etc.

2.1 Electromagnetic metamaterials

Electromagnetic metamaterials are those metamaterials which can manipulate electromagnetic waves due to its structure which is smaller than the wavelength of the wave that interacts with it. There are many types of electromagnetic metamaterials. Some of them are given below.

- **Negative-index metamaterials:** These metamaterials have negative refractive index. It means they don't follow Snell's law. Rather, the light after passing through the glass slab, gets transmitted in the same side of the slab. If permittivity and permeability both are negative for a metamaterial, then it is called a double negative metamaterial. But negative refractive index happens only for a particular frequency range of light.
- **Frequency selective surface-based metamaterials:** The name itself indicates that these metamaterials are those which are selective in nature. It means they have the ability to select a specific frequency range and make it unable to pass through while making other frequencies able to pass through.
- **Electromagnetic bandgap metamaterials:** These are those which can control light propagation. They have a bandgap, which is the range of frequencies of electromagnetic waves that cannot propagate through the material.
- **Single negative metamaterials:** These metamaterials either have negative relative permittivity or negative relative permeability.
- **Terahertz metamaterials:** These are those metamaterials that interact with terahertz frequencies (0.1 THz to 10 THz).
- **Photonic metamaterials:** These are those metamaterials which interact with mid-infrared frequencies.
- **Tunable metamaterials:** These are those metamaterials which can be tuned for certain frequencies by changing structural parameters, temperature, stretching, etc.
- **Plasmonic metamaterials:** These are those metamaterials in which when light interacts with its structure, surface plasmons (collective electron oscillations) are produced

between the metal and dielectric interface which can then be used to achieve optical properties which are not found in nature.

2.2 Elastic metamaterials

Elastic metamaterials are those metamaterials which have elastic properties such as bulk modulus, Young's modulus etc. They are also called mechanical metamaterials. These metamaterials are designed in such a way that it can show negative Poisson's ratio (auxetic metamaterials in which stretching a structure leads to increase in size in every direction and compressing a structure leads to decrease in size in every direction), negative stiffness, negative compressibility etc.

2.3 Acoustic metamaterials

These metamaterials can manipulate sound waves. For example, these can allow certain frequencies of sound waves to pass through while absorbing others.

2.4 Thermal metamaterials

These metamaterials can manipulate flow of heat. For example, if we want to make some parts of a component of a system hotter than others, we can use these metamaterials to control the flow of heat and direct it to the area where we want to make it hot.

2.5 Nonlinear metamaterials

Nonlinear metamaterials are those metamaterials which are designed to show nonlinear behavior to electromagnetic waves. It means the response is not linear, rather it is nonlinear.

3. APPLICATIONS OF METAMATERIALS

Metamaterials have many applications. They can be used to create absorbers, antennas, cloaking devices, superlens, seismic metamaterials, RCS (radar cross section) reducing metamaterials etc.

3.1 Metamaterial antennas

These are designed to increase the radiated power of antennas even if the size of antenna is small.

3.2 Metamaterial absorber

It is designed in such a way that it can absorb large amount of electromagnetic radiation. It can be used for solar photovoltaic applications because maximum energy is absorbed.

3.3 Superlens

It is a 2D or 3D device which can achieve excellent resolution due to its negative refraction properties that comes from metamaterials. It gets its high resolution because it overcomes the diffraction limit. So, it can resolve very tiny particles and provide clear image which is not possible with conventional microscope. Superlens uses the evanescent wave, which is a rapidly decaying wave at the interface, to capture detailed information about the particle that is magnified.

3.4 Cloaking device

This device is made in such a way that it bends the wave around it and let it go as if it is invisible to the wave.

3.5 Radar cross-section (RCS) reducing metamaterials

These metamaterials are fabricated such that it can minimize the detection of objects by radar systems. Basically, what it does is that it reduces the reflected light from the object which is to be made detection free. These metamaterials are particularly used in stealth technology.

3.6 Seismic metamaterials

These can be used in structures such as buildings, bridges etc. to reduce the adverse effects of seismic waves.

3.7 Acoustic metamaterials

These can be designed in such a way that it can absorb the desired sound frequencies. So, they can be used to make a place sound proof.

4. DESIGN AND METHOD

Till now, a large amount of research work has been conducted by numerous scientists in the field of metamaterials. But, what attracted my mind is the metamaterial absorbers. Using COMSOL Multiphysics simulation software, I conducted a detailed study is done on an asymmetric metamaterial absorber which has dual-band, wide-angle and polarization-independent infrared absorption for both TE and TM incidences. By studying the z-component of electric field distribution for the resonant wavelengths, it was found that the absorption of those two wavelengths is due to magnetic polariton modes excited at two different resonant wavelengths [36].

The design of the unit cell of the proposed metamaterial absorber is made using Finite Element Method (FEM) based COMSOL Multiphysics Simulation software. Illustration of the unit cell from the top and side view of the proposed design is depicted in Fig. 4.1. Copper material is used to set the bottom metal layer and the top structural design. The reason for using copper is that it is cheap and it has high conductivity of 5.998×10^7 S/m. Silicon carbide (SiC) is used to create the dielectric substrate in the middle which has dielectric constant or relative permittivity value 10.8 and loss tangent value 0.003, which makes it suitable for mid-infrared applications. Moreover, it has high thermal conductivity and can withstand high temperatures. Further, the operating range of wavelength is chosen to be from 5 μm to 10 μm which lies in the mid-infrared region. The reason for using this wavelength range is that it encompasses the low-wavelength end of the molecular fingerprint region where vibrational modes of many solids, liquids, and gases occur. Moreover, it overlaps with the Earth's atmospheric window including the peak of blackbody emission for 300 K objects, making it vital for chemical sensing and thermal imaging.

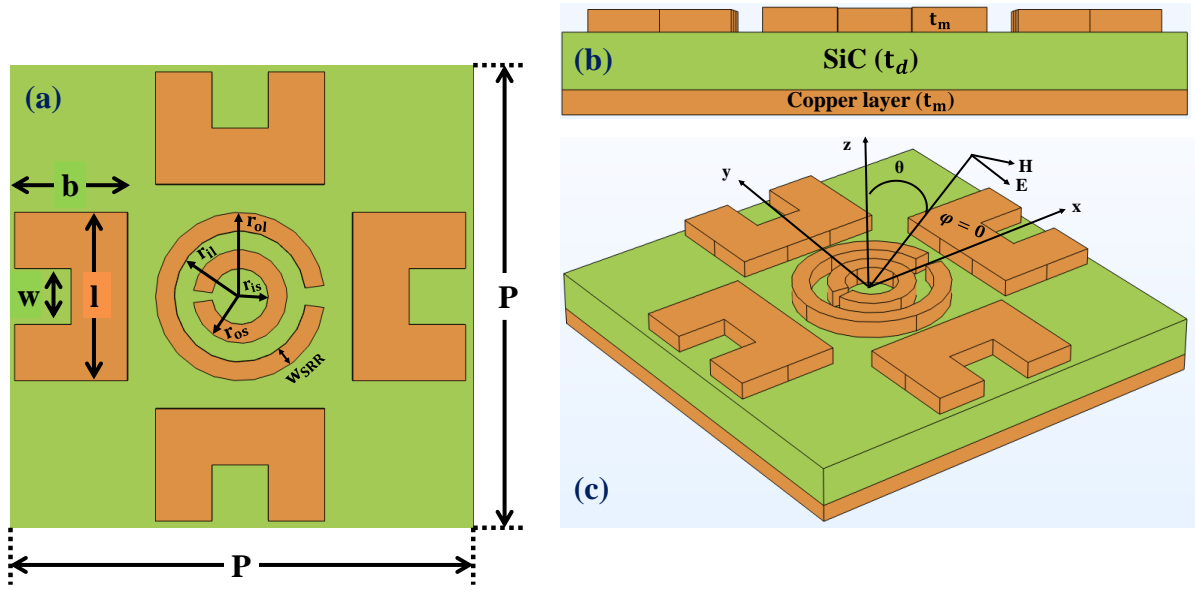


Fig. 4.1. (a) Top view, (b) side view and (c) TE wave incident on the structure from x-z plane with an incident angle of θ with z-direction and azimuthal incident angle $\phi = 0^\circ$ of the proposed unit cell of the metamaterial absorber.

The values of different geometrical parameters are given in the Table 4.1 in which P denotes lattice period, t_d denotes thickness of SiC, t_m denotes thickness of copper layer, l , b , and w denotes dimensions of C-shaped patch, r_{ol} denotes outer radius of large split-ring resonator, r_{il} denotes inner radius of large split-ring resonator, r_{os} denotes outer radius of small split-ring resonator, r_{is} denotes inner radius of smaller split-ring resonator and w_{SRR} denotes width of split-ring resonator.

Table 4.1 Unit Cell Dimension

Parameter	P	t_d	t_m	l	b	w	r_{ol}	r_{il}	r_{os}	r_{is}	w_{SRR}
Value (μm)	2.50	0.23	0.10	0.90	0.60	0.30	0.45	0.35	0.25	0.15	0.10

In Fig. 4.1 (c), consider a transverse electric (TE) wave in the x-z plane falling on the structure in which the incident wave makes angle θ with the z-axis and azimuthal incident angle (angle made by the projection of incident wave on x-y plane and x-axis) $\phi = 0^\circ$ with the x-axis. The electric field vibrations are along y-direction, and the magnetic field vibrations are in the x-z plane. Similarly, the transverse magnetic (TM) wave would have magnetic field vibrations along y-axis and electric field vibrations in x-z plane for $\phi = 0^\circ$. Boundary conditions which are periodic are used for both x- and y-directions.

The thickness of the copper layer at the bottom is chosen larger than the typical skin depth of copper so that the mid-infrared wave cannot pass through it. So, there would be no transmission of the wave through it. Thus, only reflection would be there and no transmission. The absorptivity formula is given as $A = 1 - |S_{11}|^2 - |S_{21}|^2$, in which $|S_{11}|$ denotes the absolute value of reflection coefficient and $|S_{21}|$ denotes the absolute value of transmission coefficient. But since $|S_{21}| = 0$, therefore, we are left with $A = 1 - |S_{11}|^2$. Impedance matching condition is also investigated. The formula for matching the impedance of the metamaterial absorber with that of air or vacuum when there is 0 transmission is given by $z = (1+S_{11})/(1-S_{11})$. If its real component is close to 1, and imaginary component is close to 0, it means good impedance matching is achieved. The wavelength range is chosen to be 5 μm to 10 μm which is in the mid-infrared range.

5. RESULTS AND DISCUSSION

The result of absorption spectrum of the proposed structure when infrared waves fall perpendicular to the structure is given in Fig. 5.1 with impedance matching.

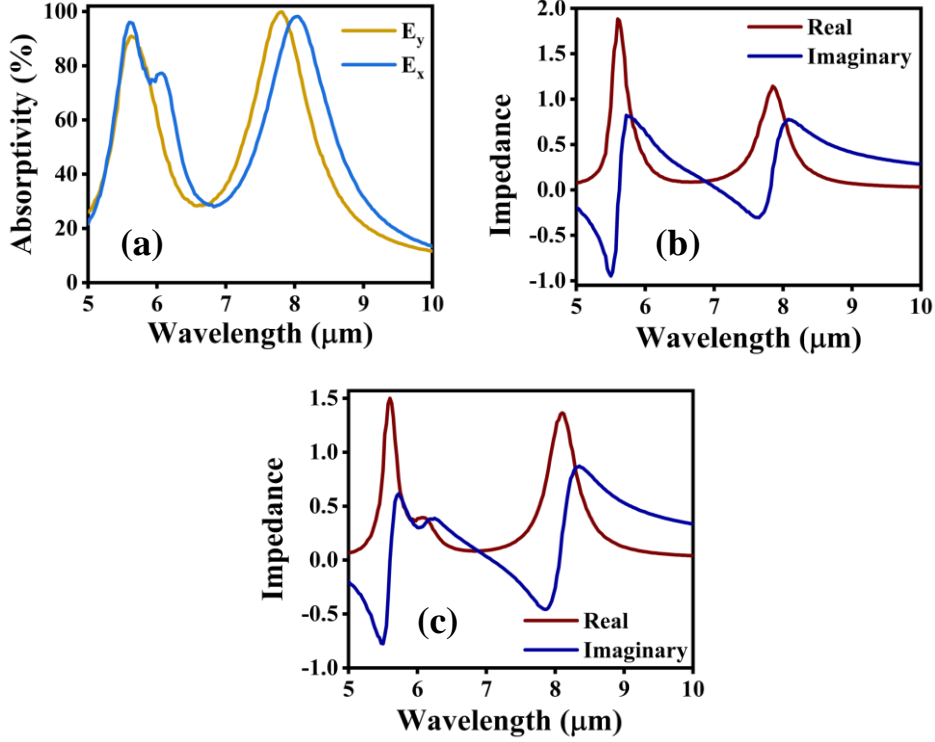


Fig. 5.1. (a) Absorption response of the designed metamaterial absorber under normal incidence ($\theta = 0^\circ$), with the electric field vibrations of the mid-infrared wave along the y-direction (E_y) and x-direction (E_x), (b) Real and imaginary components of the effective impedance for y-polarized electric field, and (c) Real and imaginary components of the effective impedance for x-polarized electric field.

Two absorption peaks reaching 90.90% at 5.62 μm and 99.86% at 7.80 μm in Fig. 5.1 (a) are observed when electric field vibrations are in y-direction, while 95.99% at 5.60 μm and 98.21% at 8.05 μm are observed when electric field vibrations are in x-direction. A slight hump can be seen in Fig. 5.1 (a) at about 6.07 μm for E_x but since its absorptivity is less as compared to the peaks, so it can be neglected. A good impedance matching of the structure and the air (or vacuum) can also be seen in Fig. 5.1 (b) and (c) in which the real component of the relative impedance is very close to 1 at the wavelengths where the absorptivity is maximum, and it helps to minimize reflection.

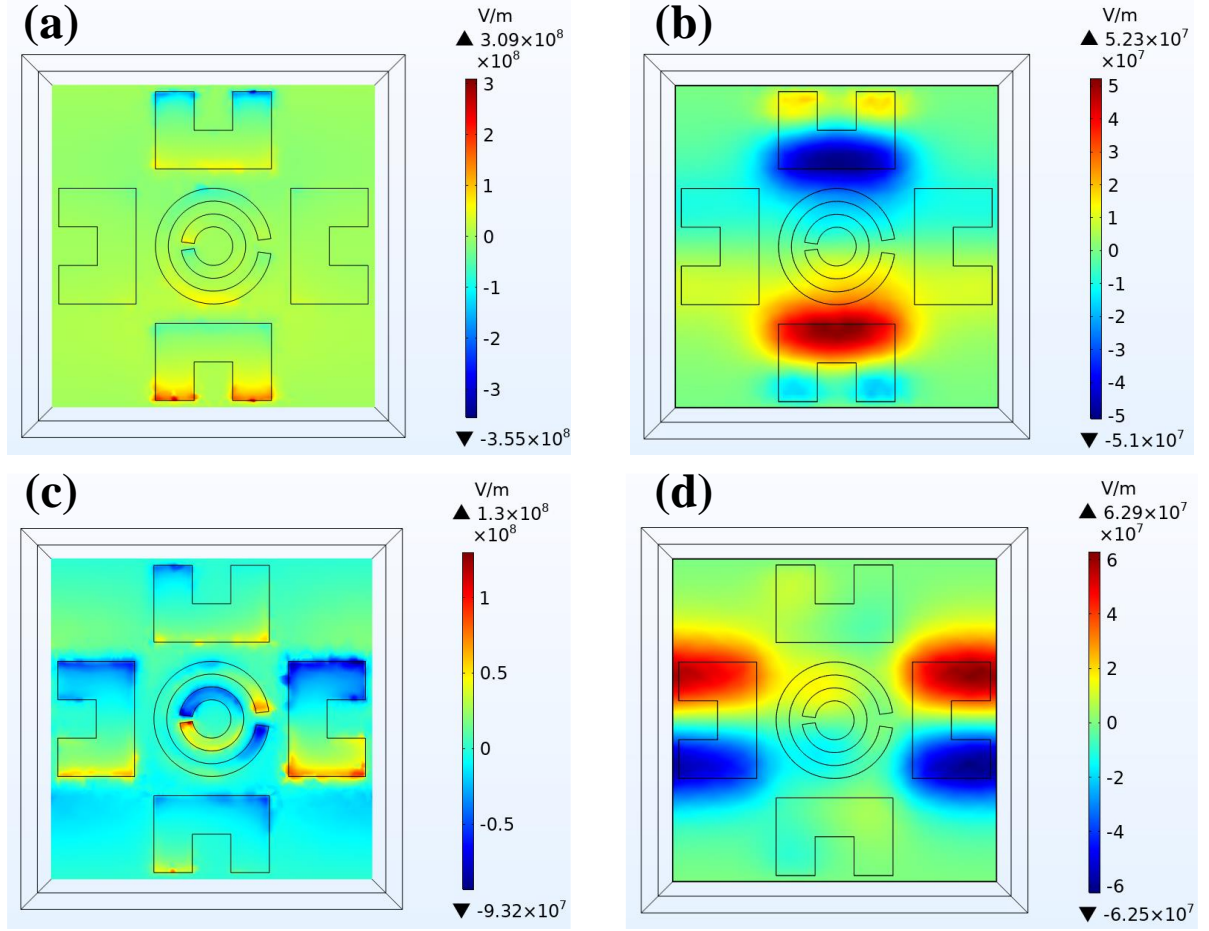


Fig. 5.2. Z-component of electric field distribution at the resonant wavelengths of 5.62 μm and 7.80 μm under normal incidence with electric field vibrations along the y-direction: (a) on the top copper layer at 5.62 μm , (b) on the bottom copper layer at 5.62 μm , (c) on the top copper layer at 7.80 μm , and (d) on the bottom copper layer at 7.80 μm .

To understand how absorption of the two wavelengths is happening, the z-component of electric field's distribution on top of the copper structure and on the copper layer at the bottom is shown in Fig. 5.2 for both the resonant wavelengths when the electric field vibrations are in y-direction. For the electric field vibrations in x-direction, the z-component of electric field distributions are given in Fig. 5.3. In Fig. 5.2 (a), for resonant wavelength 5.62 μm , we can see that the magnitude of the z-component of electric field distribution is more at the ends of C-shaped structures located in vertical direction. On the top of the copper layer at the bottom, in Fig. 5.2 (b) it is noticed that the z-component of electric field distribution is opposite in sign as compared to that on the top of the copper structural design. Moreover, in Fig. 5.2 (b), we can see two regions red and blue with a large electric field. These things mean two current loops are induced around the SiC dielectric substrate. It shows that magnetic polariton modes are excited in the copper structural design which results in magnetic resonances [36] .

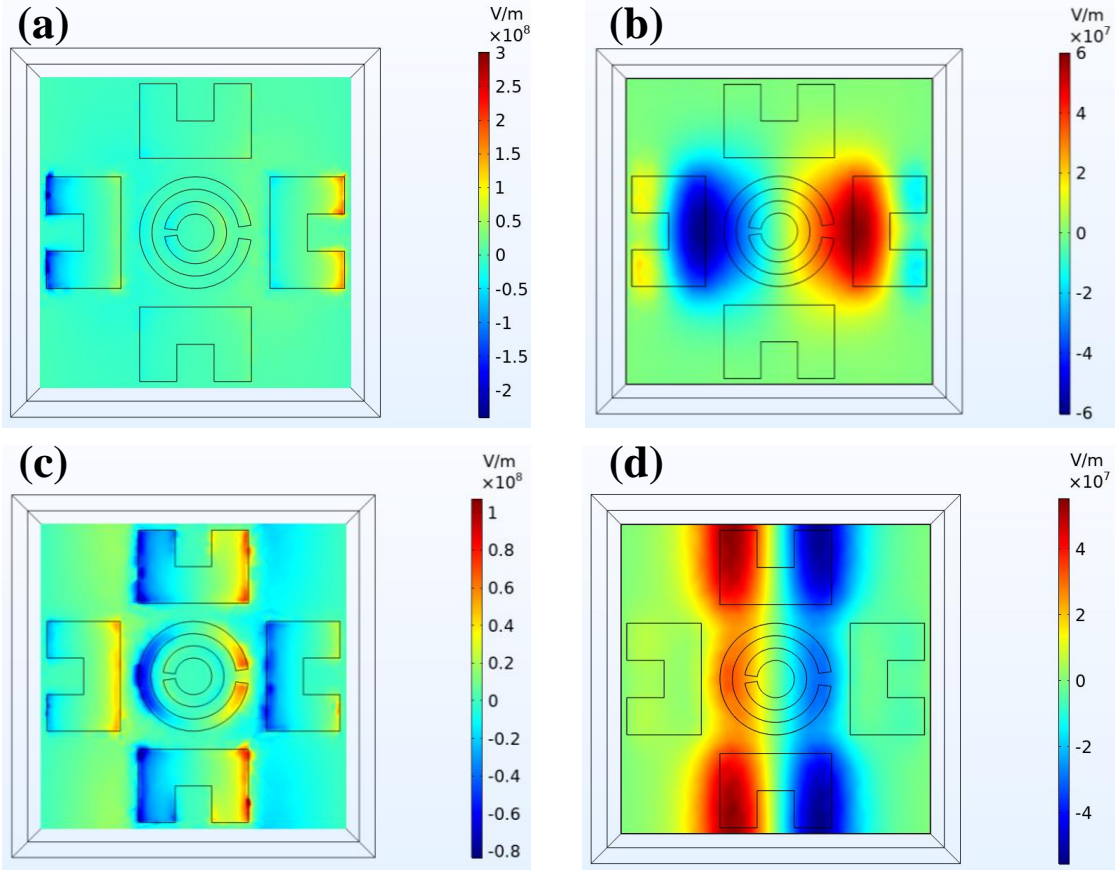


Fig. 5.3. Z-component of the electric field distribution under normal incidence with the electric field polarized along the x-direction: (a) on the top copper structure at the resonant wavelength of 5.60 μm , (b) on the bottom copper layer at 5.60 μm , (c) on the top copper structure at 8.05 μm , and (d) on the bottom copper layer at 8.05 μm .

Similarly, for the wavelength 7.80 μm , the resulting z-component of electric field distribution is shown in Fig. 5.2 (c) and (d). From (c) and (d) we can see the blue, red, and yellow regions. Red regions indicate the electric field direction towards us, and yellow regions indicate weak electric field direction towards us, and blue regions indicate electric field direction away from us. On the top of the copper layer at the bottom, in Fig. 5.2 (d) it is noticed that the z-component of electric field distribution is opposite in sign as compared to that on the top of the copper structural design. So, current loops are induced around the SiC dielectric substrate. It means absorption at the two wavelengths is occurring due to excitation of magnetic polariton modes at those wavelengths. When the electric field vibrations are in x-direction, the z-component of electric field distributions are given in Fig. 5.3. By using the same logic as given in Fig. 5.2 we can understand the cause of dual-band absorption from Fig. 5.3. Here too, the z-component of electric field distribution are opposite in direction for (a) and (b), and (c) and (d) for both resonant wavelengths, so current loops are induced around the SiC dielectric substrate. This indicates that the dual-band absorption is due to different magnetic polariton modes excited at the two wavelengths [36].

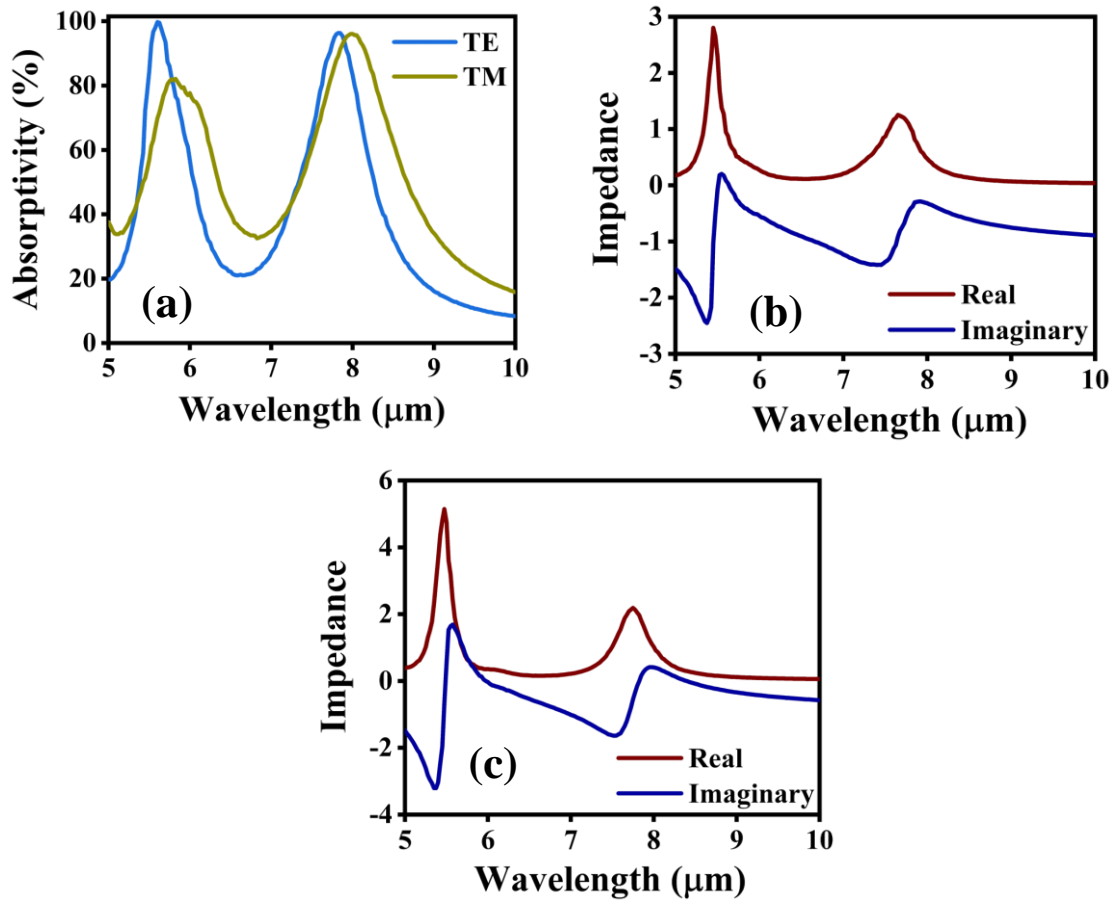


Fig. 5.4. (a) Absorption spectra of the proposed metamaterial absorber under TE and TM polarized incidence at an oblique angle ($\theta = 45^\circ$, $\phi = 0^\circ$); (b) and (c) show the corresponding real and imaginary parts of the effective impedance for TE and TM polarizations, respectively.

We have further investigated the absorption spectra of the proposed structure at incident angle $\theta = 45^\circ$ and azimuthal incident angle $\phi = 0^\circ$ for both TE and TM incidences as depicted in Fig. 5.4. The results of effective impedance are also shown. Two absorption peaks are observed reaching 99.74% at 5.60 μm wavelength, and 96.34% at 7.82 μm for TE incidence (electric field vibrations perpendicular to incident plane), while 82.09% at 5.82 μm , and 96.05% at 8.00 μm for TM incidence (magnetic field vibrations perpendicular to incident plane). For this case too, a good impedance matching of the structure and the air (or vacuum) can be noticed in Fig. 5.4 (b) and Fig. 5.4 (c) in which the real component of the relative impedance is very close to 1 at the wavelengths where the absorptivity is maximum, and it helps to minimize reflection. But, for the TM incidence, at the first peak at 5.82 μm , impedance matching is not good as can be seen in the graph in Fig. 5.4 (c). That's why, the absorptivity is low here. But still, 82.09% absorptivity is also good.

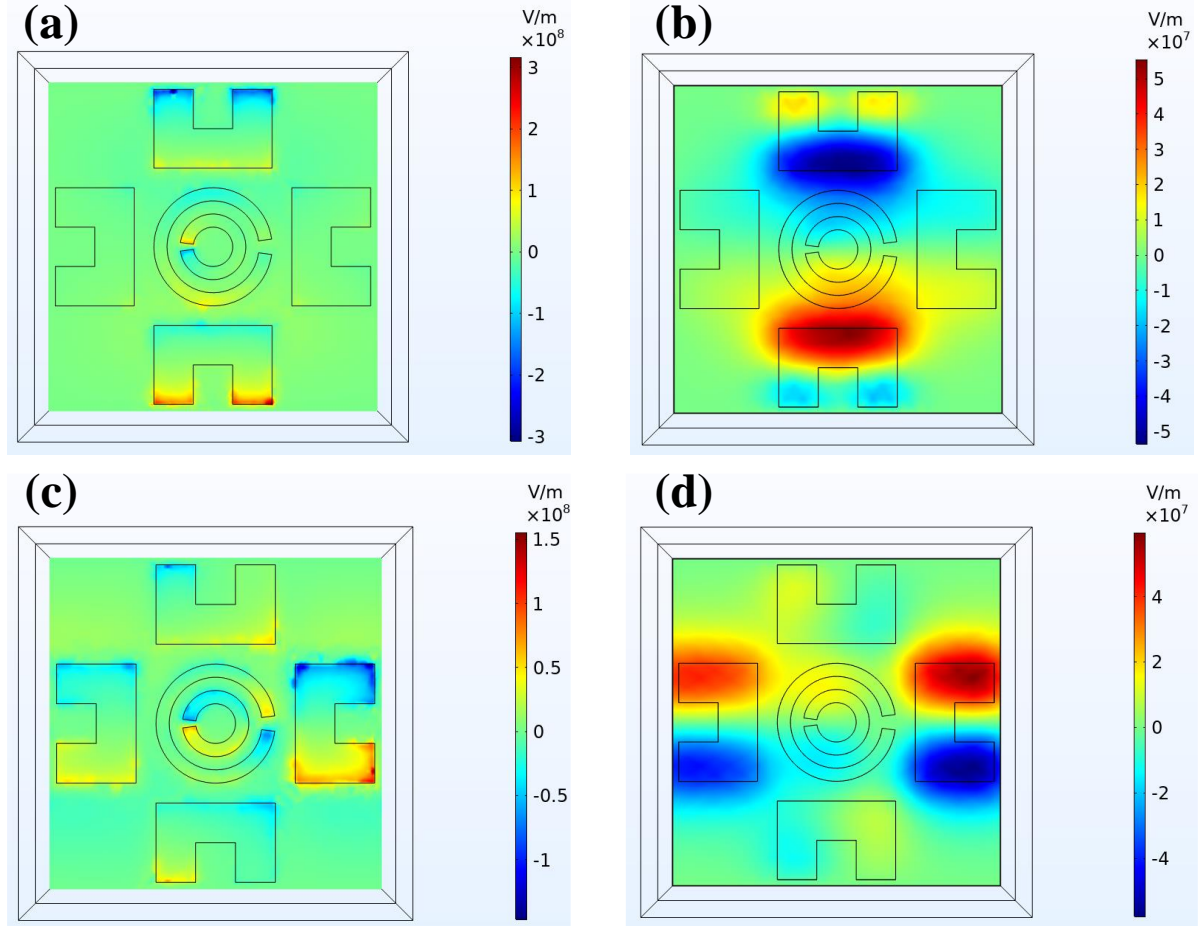


Fig. 5.5. Z-component of the electric field distribution for TE-polarized incidence at an oblique angle ($\theta = 45^\circ$, $\phi = 0^\circ$): (a) on the top copper structure and (b) on the bottom copper layer at the resonant wavelength of $5.60 \mu\text{m}$; (c) on the top copper structure and (d) on the bottom copper layer at the resonant wavelength of $7.82 \mu\text{m}$.

To understand the absorption of the two wavelengths shown in Fig. 5.4, the z-component of electric field's distribution is shown in Fig. 5.5 for TE incidence, and Fig. 5.6 for TM incidence. For both the cases, similar reasons apply as already explained before for perpendicular incidence, i.e. induced current loops are formed around the SiC dielectric substrate, and hence, excitation of different magnetic polariton modes occur at the two wavelengths [36].

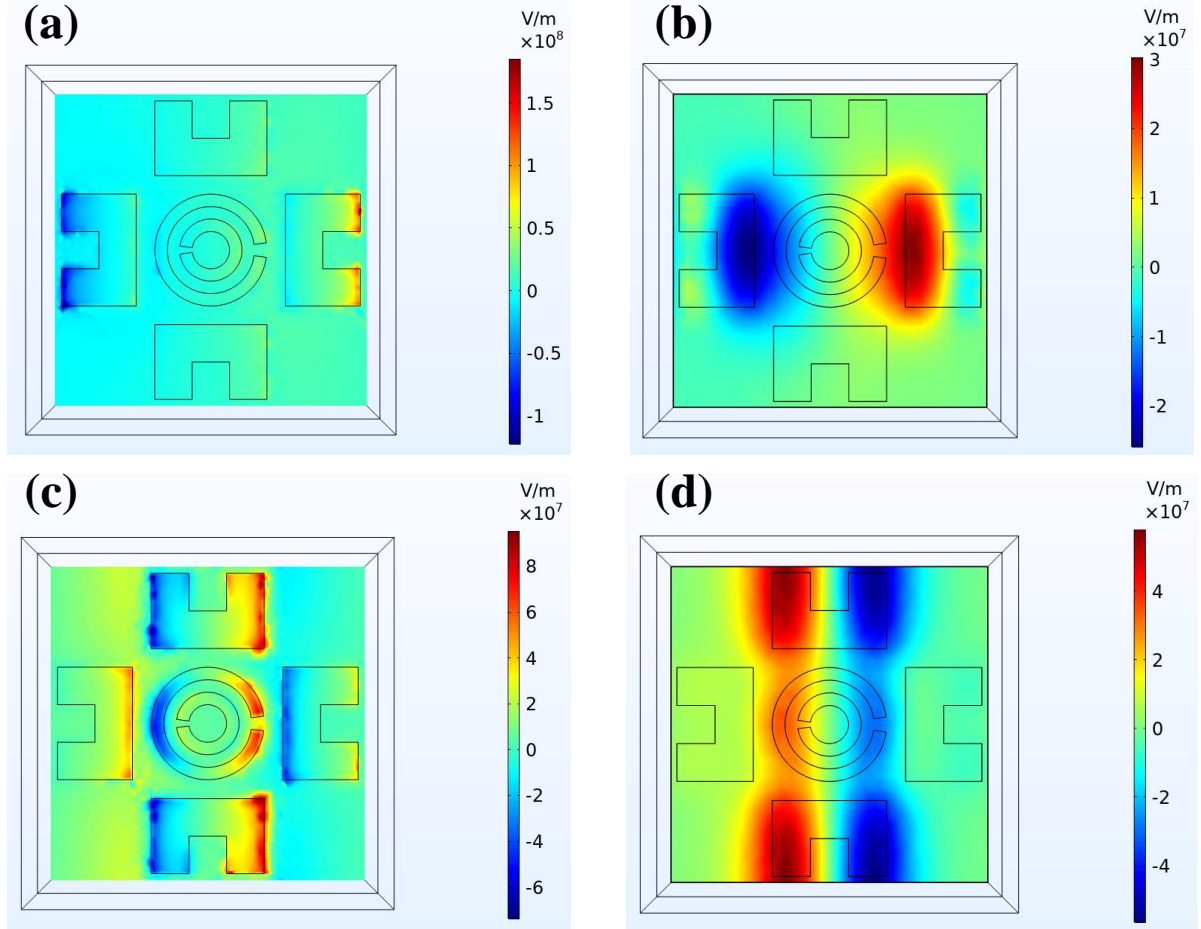


Fig. 5.6. Z-component of the electric field distribution for TM-polarized incidence at an oblique angle ($\theta = 45^\circ$, $\phi = 0^\circ$): (a) on the top copper structure and (b) on the bottom copper layer at the resonant wavelength of $5.82 \mu\text{m}$; (c) on the top copper structure and (d) on the bottom copper layer at the resonant wavelength of $8.00 \mu\text{m}$.

We have further investigated the absorption spectra of the proposed structure at incident angle $\theta = 45^\circ$ and azimuthal incident angle $\phi = 90^\circ$ for both TE and TM incident wave as depicted in Fig. 5.7. The results of effective impedance are also shown. Absorption peaks at two wavelengths are observed reaching 99.37% at $5.60 \mu\text{m}$ wavelength, and 99.28% at $8.02 \mu\text{m}$ for TE incidence, while 77.46% at $5.75 \mu\text{m}$, and 99.00% at $7.78 \mu\text{m}$ for TM incidence. A slight hump can be seen in Fig. 5.7 (a) at about $6.18 \mu\text{m}$ for TE incidence but since its absorptivity is less as compared to the peaks, it can be neglected. A good impedance matching of the structure and the air (or vacuum) can be seen in Fig. 5.7 (b) and (c) in which the real component of the impedance is very close to 1 at the wavelengths where the absorptivity is maximum, and it helps to minimize reflection. But for the TM incidence case, the first peak at lower wavelength is not high enough because the effective impedance is not close to 1 (impedance matching has not been achieved perfectly) as can be seen in the graph of Fig. 5.7 (c). Moreover, for the TM incidence case, it can be seen that there could be some other peak below the wavelength of 5

μm . But, here we are considering the operating wavelength range of 5 μm to 10 μm only for the reason as already described before.

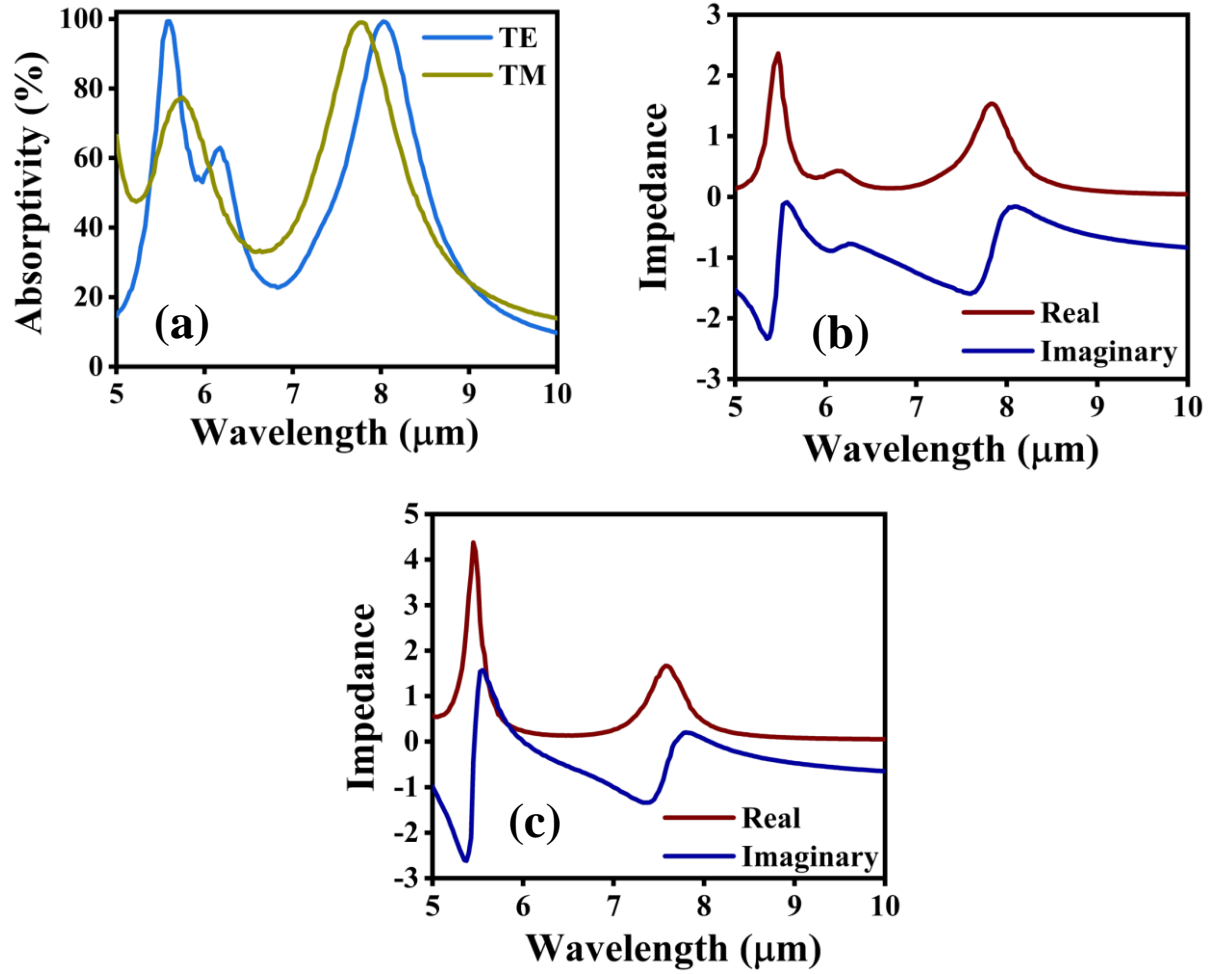


Fig. 5.7. (a) Absorption spectra of the proposed metamaterial absorber under TE and TM polarized incidence at an oblique angle ($\theta = 45^\circ$, $\phi = 90^\circ$); (b) and (c) show the corresponding real and imaginary components of the effective impedance for TE and TM polarizations, respectively.

To understand the absorption of the two wavelengths shown in Fig. 5.7, the z-component of electric field's distribution is shown in Fig. 5.8 for TE incidence, and Fig. 5.9 for TM incidence. For both the cases, similar reasons apply as already explained before for perpendicular incidence i.e. induced current loops are formed around the SiC dielectric substrate, and hence, excitation of different magnetic polariton modes occur at the two wavelengths [36].

For the TM incidence case in Fig. 5.9 (a) and (b), the z-component of electric field's distribution is slightly different if we compare it with all other results shown previously. The reason is that magnetic polariton modes are not excited properly. In simple tabular form, the results of the absorptivity are given in Table 5.1.

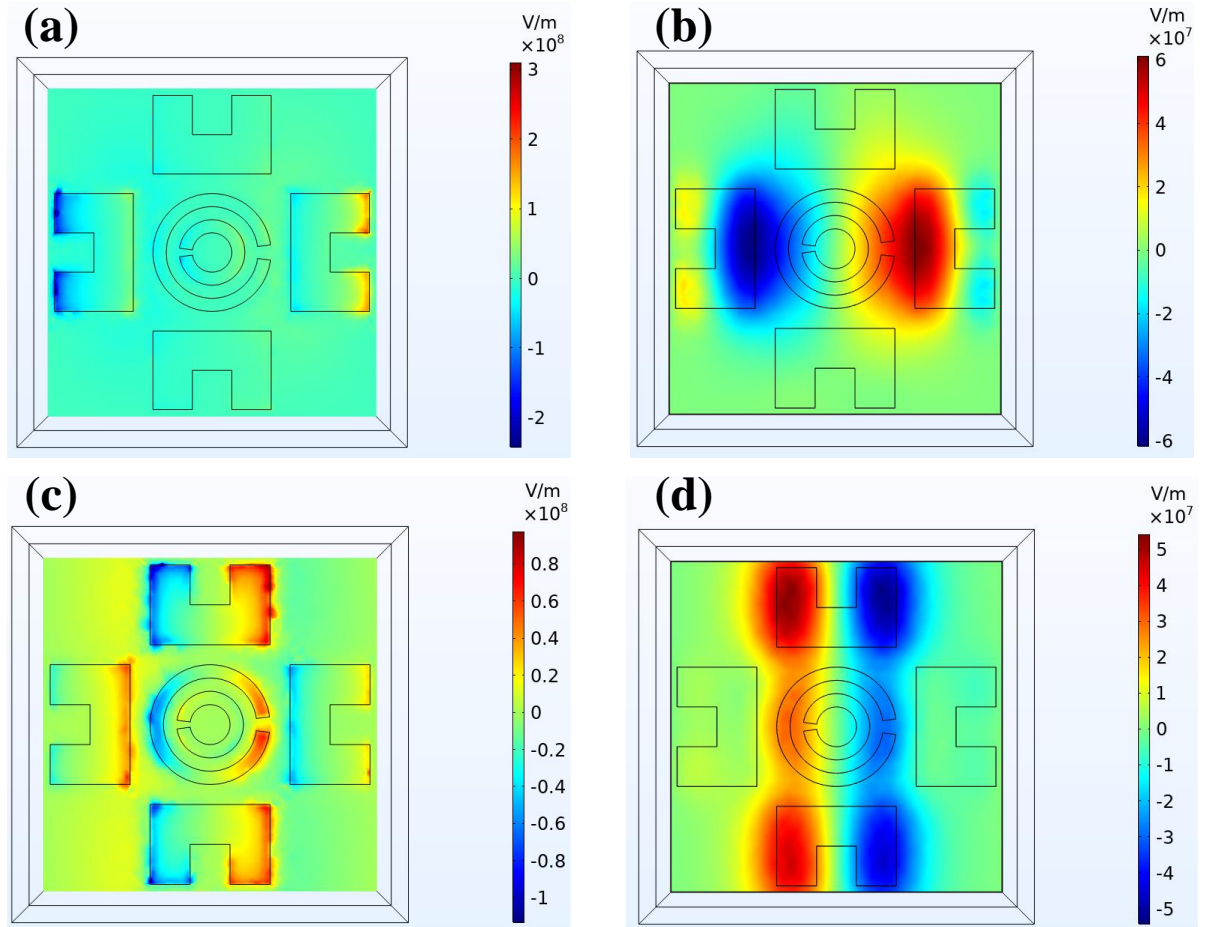


Fig. 5.8. Z-component of the electric field distribution for TE-polarized incidence at an oblique angle ($\theta = 45^\circ$, $\phi = 90^\circ$): (a) on the top copper structure and (b) on the bottom copper layer at the resonant wavelength of $5.60 \mu\text{m}$; (c) on the top copper structure and (d) on the bottom copper layer at the resonant wavelength of $8.02 \mu\text{m}$.

Table 5.1 Dual-band absorption at different incident angles

Angle of incidence	Absorptivity at first peak	Absorptivity at second peak
$\theta = 0^\circ$, Electric field vibrations in y-direction	90.90% at $5.62 \mu\text{m}$	99.86% at $7.80 \mu\text{m}$
$\theta = 0^\circ$, Electric field vibrations in x-direction	95.99% at $5.60 \mu\text{m}$	98.21% at $8.05 \mu\text{m}$
$\theta = 45^\circ$, $\phi = 0^\circ$, TE incidence	99.74% at $5.60 \mu\text{m}$	96.34% at $7.82 \mu\text{m}$
$\theta = 45^\circ$, $\phi = 0^\circ$, TM incidence	82.09% at $5.82 \mu\text{m}$	96.05% at $8.00 \mu\text{m}$
$\theta = 45^\circ$, $\phi = 90^\circ$, TE incidence	99.37% at $5.60 \mu\text{m}$	99.28% at $8.02 \mu\text{m}$
$\theta = 45^\circ$, $\phi = 90^\circ$, TM incidence	77.46% at $5.75 \mu\text{m}$	99.00% at $7.78 \mu\text{m}$

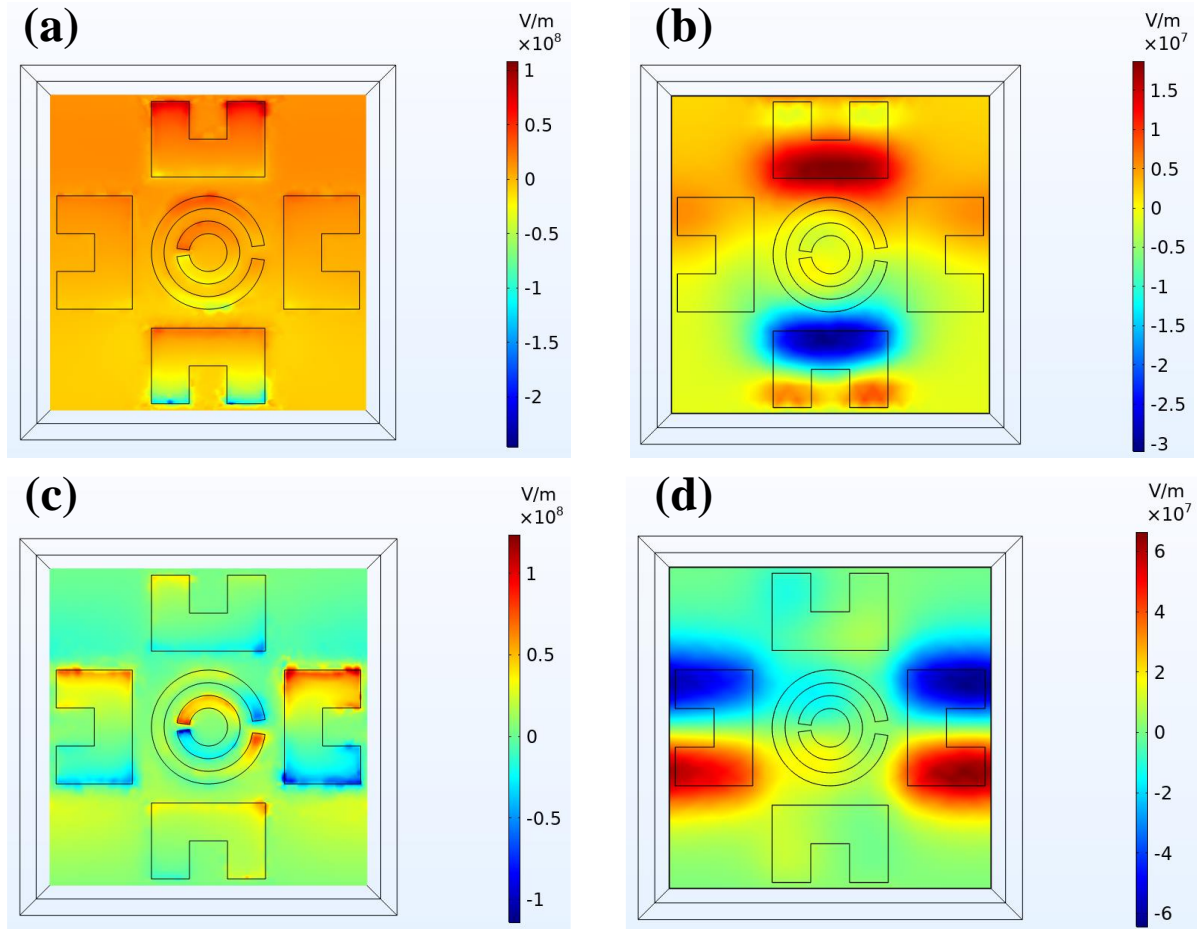


Fig. 5.9. Z-component of the electric field distribution for TM-polarized incidence at an oblique angle ($\theta = 45^\circ$, $\phi = 90^\circ$): (a) on the top copper structure and (b) on the bottom copper layer at the resonant wavelength of $5.75 \mu\text{m}$; (c) on the top copper structure and (d) on the bottom copper layer at the resonant wavelength of $7.78 \mu\text{m}$.

Investigation of the stability of absorption of the two wavelengths with incident angle θ varying from 0° to 80° at $\phi = 0^\circ$ was carried out as shown in Fig. 5.10 (a) and (b) for TE incidence, and in Fig. 5.10 (c) and (d) for TM incidence. In TE incidence, a dual-band absorption of about more than 85% is achieved when θ varies from 0° to 60° . For larger than 60° , the absorption peaks drop. The reason is that a magnetic field's component should exist in the x-y plane for the excitation of magnetic polaritons. But, here the magnetic field which is in the x-y plane is $H \cos(\theta)$, (H denotes the magnetic field's intensity), and since the magnetic field's intensity reduces quickly at $\theta > 60^\circ$, therefore, there is a weak resonance of magnetic fields, and hence magnetic polariton modes are not excited efficiently. In TM incidence, for some reason, the absorptivity of smaller wavelength is only good for about 0° to 30° . And there is a blue shift too which is outside the operating wavelength range for this study. The absorptivity of the larger wavelength is more than 85% when θ varies from 0° to 80° . The reason is that the magnetic field vibrations are in the x-y plane for TM incidence for the whole range of $\theta = 0^\circ$

to $\theta = 80^\circ$. In addition, there is a blue shift of the two absorption peaks as θ tends to larger value because of the off-phase oscillating effect in each unit cell [29].

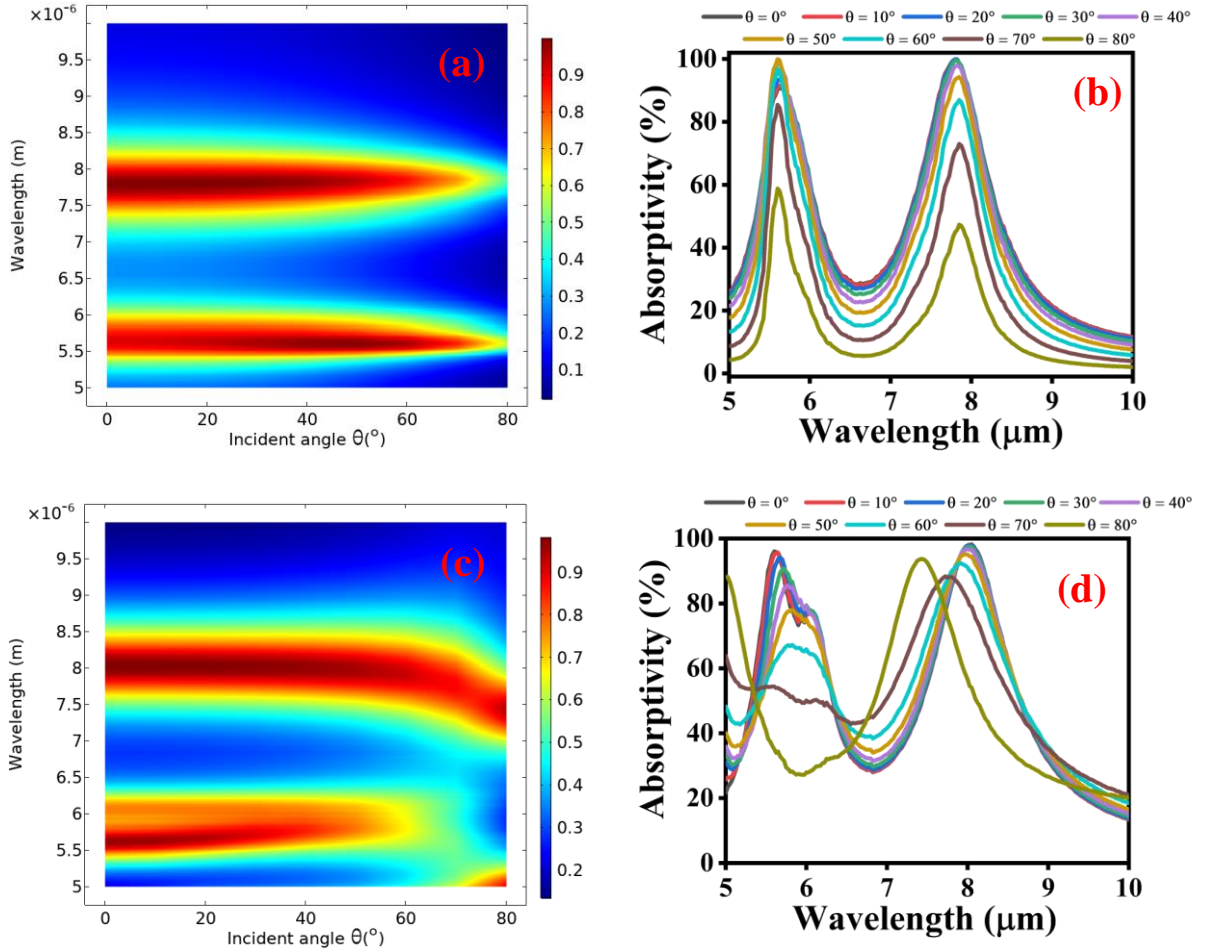


Fig. 5.10. Absorption spectra of the proposed metamaterial absorber as the incident angle (θ) varies from 0° to 80° at $\phi = 0^\circ$: (a) for TE-polarized incidence, (b) corresponding colormap representation for TE incidence, (c) for TM-polarized incidence, and (d) corresponding colormap representation for TM incidence. Absorption intensity is illustrated using the colormap scale.

Investigation of the stability of absorption of the two wavelengths with incident angle θ varying from 0° to 80° at $\phi = 90^\circ$ is also carried out as shown in Fig. 5.11 (a) and (b) for TE incidence, and in Fig. 5.11 (c) and (d) for TM incidence. In TE incidence, a dual-band absorption of about more than 90% is achieved when θ varies from 0° to 60° . For larger than 60° , the absorption peaks drop. The reason is that a magnetic field's component should exist in x-y plane for the excitation of magnetic polaritons. But here the magnetic field which is in the x-y plane is $H \cos(\theta)$, (H denotes the magnetic field's intensity), and since the magnetic field's intensity reduces quickly at $\theta > 60^\circ$, therefore, there is a weak resonance of magnetic fields, and hence magnetic polariton modes are not excited efficiently. In TM incidence, for some reason, the absorptivity of smaller wavelength is only good for about 0° to 30° , but it is less as compared to the previous case of $\phi = 0^\circ$. And there is a blue shift too which is outside the operating

wavelength range for this study. The absorptivity of the larger wavelength is more than 95% when θ varies from 0° to 80° . The reason is that the magnetic field vibrations are in the x-y plane for TM incidence for the whole range of $\theta = 0^\circ$ to $\theta = 80^\circ$. In addition, there is a blue shift of the two absorption peaks as θ tends to larger value because of the off-phase oscillating effect in each unit cell [29].

Table 5.2 Range of θ in which absorptivity is satisfactory

Range	Absorptivity at first peak	Absorptivity at second peak
At $\phi = 0^\circ$, $\theta = 0^\circ$ to 80° in TE incidence	More than 90% for $\theta = 0^\circ$ to 60°	More than 93% for $\theta = 0^\circ$ to 50°
At $\phi = 0^\circ$, $\theta = 0^\circ$ to 80° in TM incidence	More than 90% for $\theta = 0^\circ$ to 30°	More than 95% for $\theta = 0^\circ$ to 50°
At $\phi = 90^\circ$, $\theta = 0^\circ$ to 80° in TE incidence	More than 90% for $\theta = 0^\circ$ to 60°	More than 90% for $\theta = 0^\circ$ to 60°
At $\phi = 90^\circ$, $\theta = 0^\circ$ to 80° in TM incidence	More than 84% for $\theta = 0^\circ$ to 30°	More than 96% for $\theta = 0^\circ$ to 60°

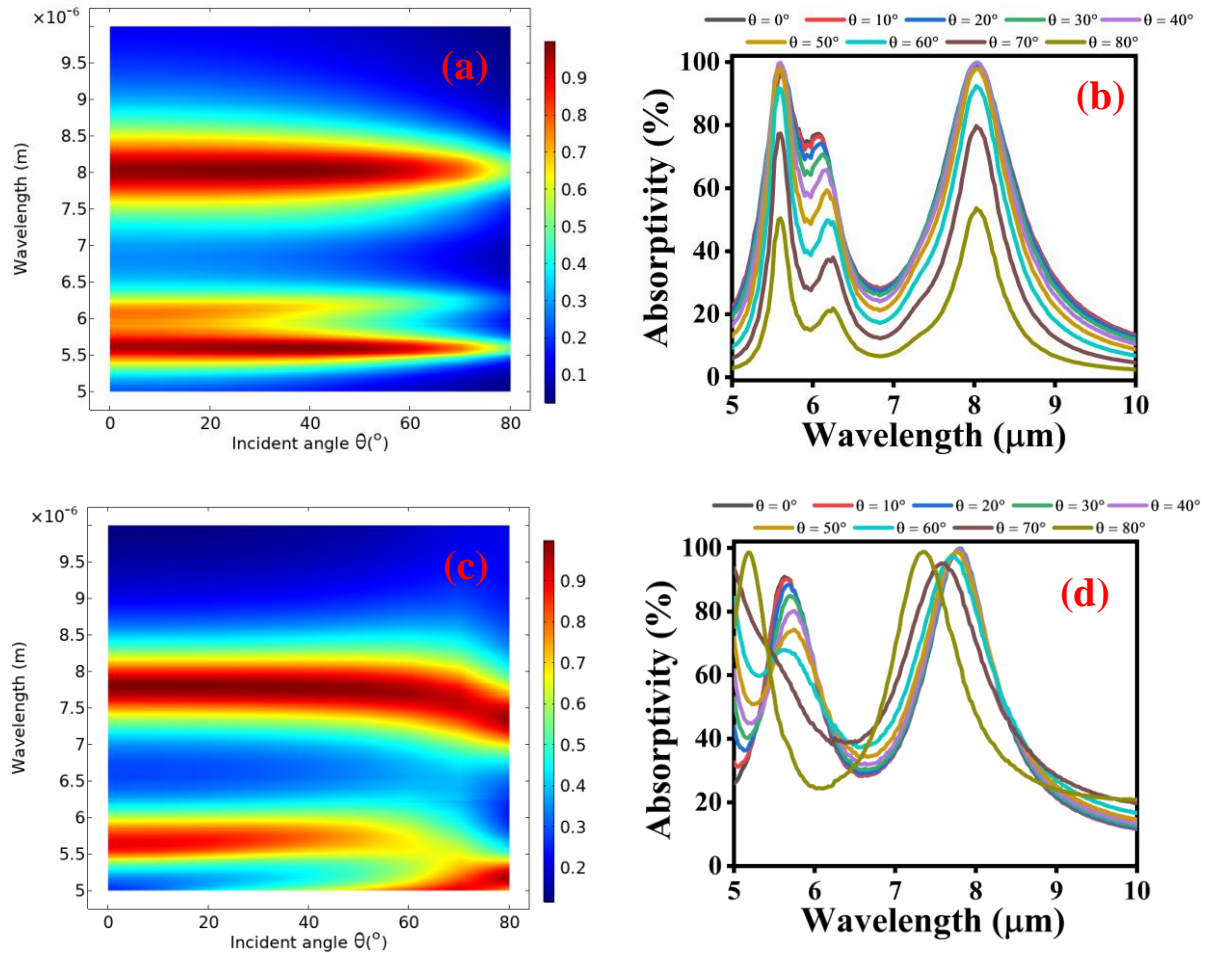


Fig. 5.11. Absorption spectra of the proposed metamaterial absorber as the incident angle (θ) varies from 0° to 80° at $\phi = 90^\circ$: (a) for TE incidence, (b) corresponding colormap representation for TE incidence, (c) for TM incidence, and (d) corresponding colormap representation for TM incidence. Absorption intensity is illustrated using the colormap scale.

Next, the results of the stability of absorptions of the two wavelengths at $\theta = 45^\circ$ with azimuthal incident angles $\phi = 0^\circ$ to 180° are given in Fig. 5.12 (a), (b), (c), (d) for TE incidence, and Fig. 5.13 (a), (b), (c), (d) for TM incidence. It can be noticed that the absorptivity of the two absorption peaks is stable as ϕ varies from 0° to 180° for both TE and TM incidences. According to Fig. 5.12, for the TE incidence case, the absorptivity of the smaller resonant wavelength is above 97% and that of the larger resonant wavelength is above 95% for the whole range of $\phi = 0^\circ$ to 180° . According to Fig. 5.13, for the TM incidence case, the absorptivity of the smaller resonant wavelength is above 76% and that of the larger resonant wavelength is above 95% for the whole range of $\phi = 0^\circ$ to 180° . The absorption by the proposed structure is insensitive with ϕ because magnetic polaritons perpendicular to each other are produced within the proposed structure at the resonant wavelengths [36]. For TE incidence, there is a small peak at the right side of the first peak as can be seen in Fig. 5.12 (b) and (d), but that can be neglected because it is small as compared to the first peak. For TM incidence, the first peak is small as depicted in Fig. 5.13 (b) and (d) because the magnetic polaritons are not excited efficiently.

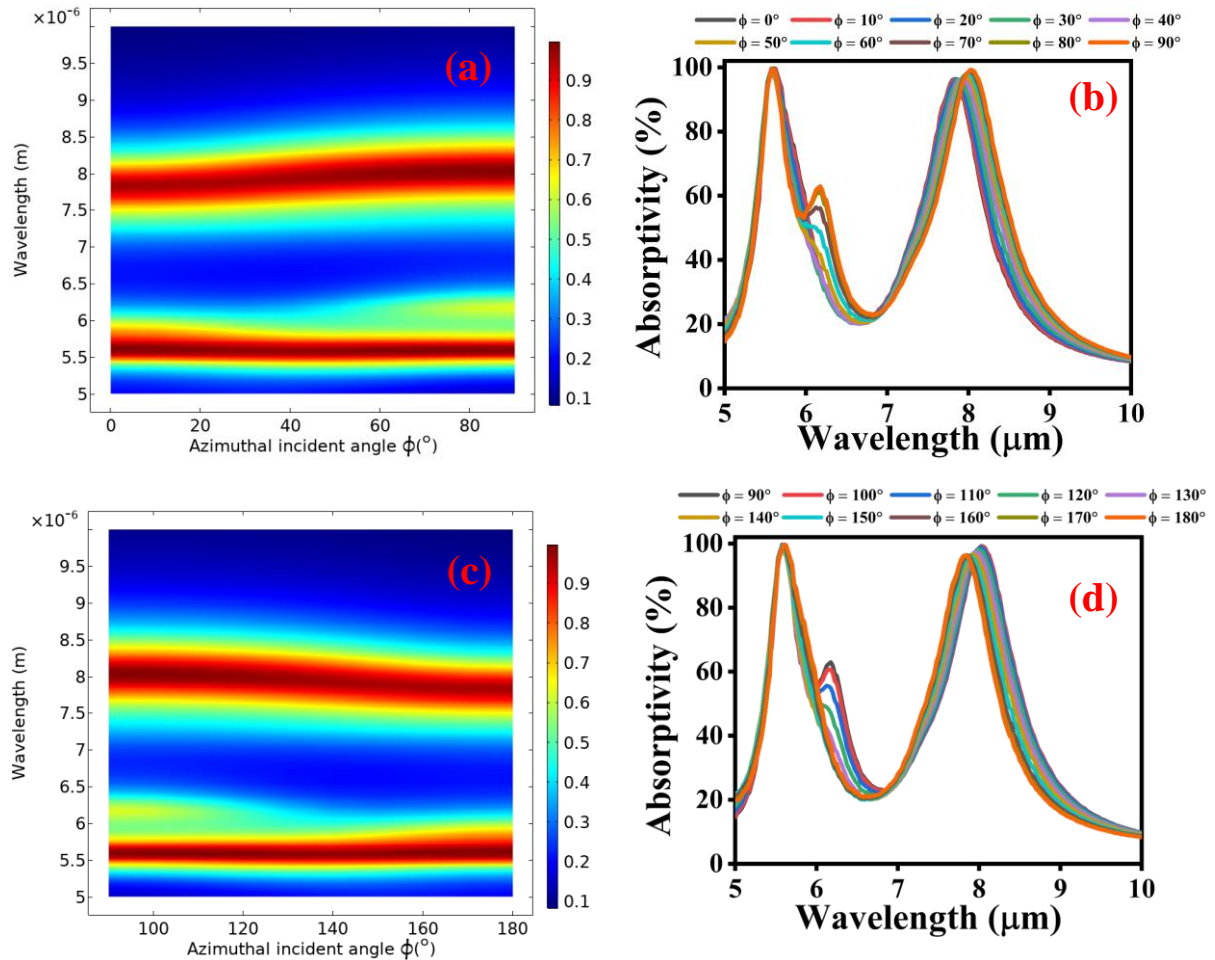


Fig. 5.12. Absorption spectra for TE-polarized incidence at $\theta = 45^\circ$ as the azimuthal angle (ϕ) varies: (a) from 0° to 90° , (b) corresponding colormap representation for $\phi = 0^\circ$ to 90° , (c) from 90° to 180° , and (d) corresponding colormap representation for $\phi = 90^\circ$ to 180° . Absorption intensity is represented by the colormap.

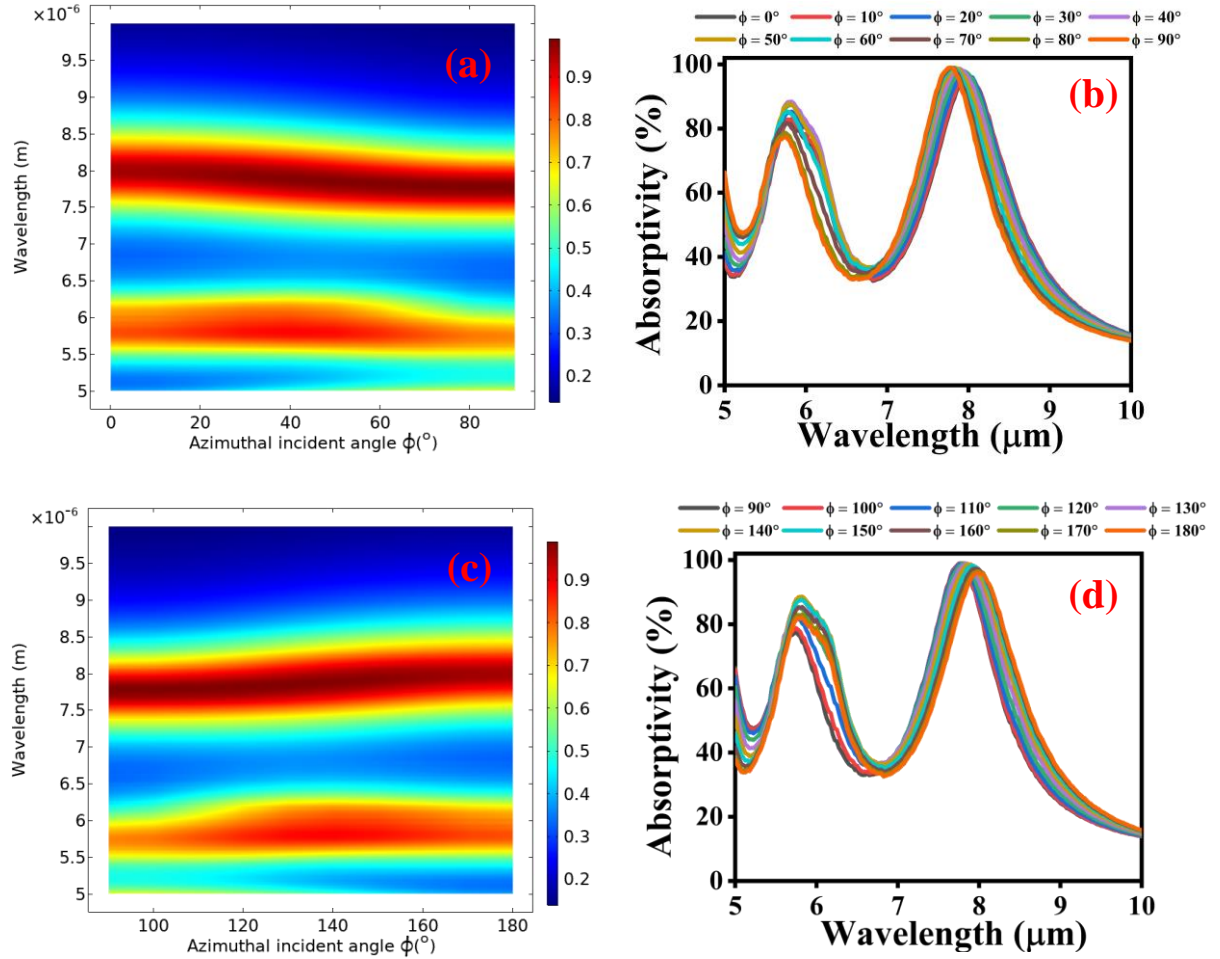


Fig. 5.13. Absorption spectra for TM-polarized incidence at $\theta = 45^\circ$ as the azimuthal angle (ϕ) varies: (a) from 0° to 90° , (b) corresponding colormap representation for $\phi = 0^\circ$ to 90° , (c) from 90° to 180° , and (d) corresponding colormap representation for $\phi = 90^\circ$ to 180° . Absorption intensity is represented by the colormap.

The results of Fig. 5.10 and Fig. 5.11 are given in Table 5.2. And the results of Fig. 5.12 and Fig. 5.13 are given in Table 5.3.

Table 5.3 Range of ϕ in which absorptivity is satisfactory

Range	Absorptivity at first peak	Absorptivity at second peak
At $\theta = 45^\circ$, $\phi = 0^\circ$ to 180° in TE incidence	More than 97% for the whole range $\phi = 0^\circ$ to 180°	More than 95% for the whole range $\phi = 0^\circ$ to 180°
At $\theta = 45^\circ$, $\phi = 0^\circ$ to 180° in TM incidence	More than 76% for the whole range $\phi = 0^\circ$ to 180°	More than 95% for the whole range $\phi = 0^\circ$ to 180°

6. CONCLUSION

An asymmetric metamaterial absorber is proposed which shows dual-band absorption in the infrared wavelength range 5 μm to 10 μm . The absorber consists of a SiC dielectric layer sandwiched between an asymmetric structure made of copper and a copper ground. Z-component of electric field distribution has also been studied for the copper structure at the top and on the bottom copper layer which showed that the absorption of the two wavelengths is due to magnetic polariton modes produced at those wavelengths. Impedance matching has also been studied. Moreover, the proposed metamaterial absorber also exhibits good absorption stability for a broad range of azimuthal incident angles ϕ and incident angles θ for both TE and TM incidence (especially for TE incidence). The absorption by the proposed structure is insensitive with ϕ because magnetic polaritons perpendicular to each other are produced within the proposed structure at the resonant wavelengths. So, the proposed metamaterial absorber can have potential applications in chemical sensing, thermal detectors, and infrared imaging.

References

- [1] D.R. Smith, J.B. Pendry, M.C.K. Wiltshire, Metamaterials and Negative Refractive Index, *Science* (80-.). 305 (2004) 788–792. <https://doi.org/10.1126/science.1096796>.
- [2] R.A. Shelby, D.R. Smith, S. Schultz, Experimental Verification of a Negative Index of Refraction, *Science* (80-.). 292 (2001) 77–79. <https://doi.org/10.1126/science.1058847>.
- [3] J. Valentine, S. Zhang, T. Zentgraf, E. Ulin-Avila, D.A. Genov, G. Bartal, X. Zhang, Three-dimensional optical metamaterial with a negative refractive index, *Nature*. 455 (2008) 376–379. <https://doi.org/10.1038/nature07247>.
- [4] K. Kishor, M.N. Baitha, R.K. Sinha, B. Lahiri, Tunable negative refractive index metamaterial from V-shaped SRR structure: fabrication and characterization, *J. Opt. Soc. Am. B*. 31 (2014) 1410. <https://doi.org/10.1364/josab.31.001410>.
- [5] J.B. Pendry, Negative Refraction Makes a Perfect Lens, *Phys. Rev. Lett.* 85 (2000) 3966–3969. <https://doi.org/10.1103/PhysRevLett.85.3966>.
- [6] W. Cai, U.K. Chettiar, A. V. Kildishev, V.M. Shalaev, Optical cloaking with metamaterials, *Nat. Photonics*. 1 (2007) 224–227. <https://doi.org/10.1038/nphoton.2007.28>.
- [7] N.I. Landy, S. Sajuyigbe, J.J. Mock, D.R. Smith, W.J. Padilla, Perfect Metamaterial Absorber, *Phys. Rev. Lett.* 100 (2008) 207402. <https://doi.org/10.1103/PhysRevLett.100.207402>.
- [8] Ankit, K. Kishor, R.K. Sinha, Design and analysis of wavelength tunable metamaterial reflector, *Results Opt.* 10 (2023) 100366. <https://doi.org/10.1016/j.rio.2023.100366>.
- [9] Ankit, K. Kishor, R.K. Sinha, SOI Based metasurface for broadband perfect reflection in visible spectrum, *J. Opt.* 26 (2024) 045101. <https://doi.org/10.1088/2040-8986/ad2bab>.
- [10] Ankit, K. Kishor, R.K. Sinha, Design, fabrication, and characterization of epsilon negative and near-zero index metasurface, *Appl. Phys. A Mater. Sci. Process.* 130 (2024) 1–15. <https://doi.org/10.1007/s00339-023-07239-z>.
- [11] K. Kishor, M.N. Baitha, R.K. Sinha, Design and simulation of “i” shaped split ring resonator metamaterial at optical communication window around 1.55 μm , *Optik (Stuttg)*. 126 (2015) 4708–4711. <https://doi.org/10.1016/j.ijleo.2015.08.086>.
- [12] Y. Qiu Xu, P. Heng Zhou, H. Bin Zhang, L. Chen, L. Jiang Deng, A wide-angle planar metamaterial absorber based on split ring resonator coupling, *J. Appl. Phys.* 110 (2011). <https://doi.org/10.1063/1.3622675>.

- [13] F. Ding, Y. Cui, X. Ge, Y. Jin, S. He, Ultra-broadband microwave metamaterial absorber, *Appl. Phys. Lett.* 100 (2012). <https://doi.org/10.1063/1.3692178>.
- [14] . A., K. Kishor, R.K. Sinha, Design and analysis of multiband metamaterial in microwave regime, in: K. Staliūnas, V. Kuzmiak, T. Stefaniuk (Eds.), *Metamaterials XIV*, SPIE, 2023: p. 33. <https://doi.org/10.1117/12.2664671>.
- [15] Ankit, K. Kishor, R.K. Sinha, ENZ metamaterial for X-band in the microwave regime, in: *Front. Opt. + Laser Sci. 2022 (FIO, LS)*, Optica Publishing Group, Washington, D.C., 2022: p. JT4B.60. <https://doi.org/10.1364/FIO.2022.JT4B.60>.
- [16] C. Hu, Z. Zhao, X. Chen, X. Luo, Realizing near-perfect absorption at visible frequencies, *Opt. Express.* 17 (2009) 11039. <https://doi.org/10.1364/OE.17.011039>.
- [17] J. Hao, J. Wang, X. Liu, W.J. Padilla, L. Zhou, M. Qiu, High performance optical absorber based on a plasmonic metamaterial, *Appl. Phys. Lett.* 96 (2010). <https://doi.org/10.1063/1.3442904>.
- [18] N. Liu, M. Mesch, T. Weiss, M. Hentschel, H. Giessen, Infrared Perfect Absorber and Its Application As Plasmonic Sensor, *Nano Lett.* 10 (2010) 2342–2348. <https://doi.org/10.1021/nl9041033>.
- [19] X. Liu, T. Tyler, T. Starr, A.F. Starr, N.M. Jokerst, W.J. Padilla, Taming the Blackbody with Infrared Metamaterials as Selective Thermal Emitters, *Phys. Rev. Lett.* 107 (2011) 045901. <https://doi.org/10.1103/PhysRevLett.107.045901>.
- [20] W.L. Barnes, A. Dereux, T.W. Ebbesen, Surface plasmon subwavelength optics, *Nature.* 424 (2003) 824–830. <https://doi.org/10.1038/nature01937>.
- [21] Ankit, M.N. Baitha, K. Kishor, R.K. Sinha, Quadrupole mode plasmon resonance enabled dual-band metamaterial for refractive index sensing application, *J. Appl. Phys.* 136 (2024). <https://doi.org/10.1063/5.0201422>.
- [22] Ankit, K. Kishor, R.K. Sinha, Design of wide bandwidth metamaterial for biosensor and wireless application, *Phys. Scr.* 100 (2025) 035503. <https://doi.org/10.1088/1402-4896/adadad>.
- [23] X. Liu, T. Starr, A.F. Starr, W.J. Padilla, Infrared Spatial and Frequency Selective Metamaterial with Near-Unity Absorbance, *Phys. Rev. Lett.* 104 (2010) 207403. <https://doi.org/10.1103/PhysRevLett.104.207403>.
- [24] P.R. Christensen, B.M. Jakosky, H.H. Kieffer, M.C. Malin, H.Y. McSween, Jr., K. Nealon, G.L. Mehall, S.H. Silverman, S. Ferry, M. Caplinger, M. Ravine, The Thermal Emission Imaging System (THEMIS) for the Mars 2001 Odyssey Mission, *Space Sci. Rev.* 110 (2004) 85–130. <https://doi.org/10.1023/B:SPAC.0000021008.16305.94>.

- [25] K. Chen, R. Adato, H. Altug, Dual-Band Perfect Absorber for Multispectral Plasmon-Enhanced Infrared Spectroscopy, *ACS Nano*. 6 (2012) 7998–8006. <https://doi.org/10.1021/nn3026468>.
- [26] Ankit, K. Kishor, R.K. Sinha, Design and analysis of a far-infrared metamaterial perfect absorber with sensing applications, *Appl. Opt.* 63 (2024) 8994. <https://doi.org/10.1364/AO.538864>.
- [27] B. Zhang, Y. Zhao, Q. Hao, B. Kiraly, I.-C. Khoo, S. Chen, T.J. Huang, Polarization-independent dual-band infrared perfect absorber based on a metal-dielectric-metal elliptical nanodisk array, *Opt. Express*. 19 (2011) 15221. <https://doi.org/10.1364/OE.19.015221>.
- [28] H. Tao, C.M. Bingham, D. Pilon, K. Fan, A.C. Strikwerda, D. Shrekenhamer, W.J. Padilla, X. Zhang, R.D. Averitt, A dual band terahertz metamaterial absorber, *J. Phys. D: Appl. Phys.* 43 (2010) 225102. <https://doi.org/10.1088/0022-3727/43/22/225102>.
- [29] Y.Q. Ye, Y. Jin, S. He, Omnidirectional, polarization-insensitive and broadband thin absorber in the terahertz regime, *J. Opt. Soc. Am. B*. 27 (2010) 498. <https://doi.org/10.1364/JOSAB.27.000498>.
- [30] P. Bouchon, C. Koechlin, F. Pardo, R. Haïdar, J.-L. Pelouard, Wideband omnidirectional infrared absorber with a patchwork of plasmonic nanoantennas, *Opt. Lett.* 37 (2012) 1038. <https://doi.org/10.1364/OL.37.001038>.
- [31] C.-W. Cheng, M.N. Abbas, C.-W. Chiu, K.-T. Lai, M.-H. Shih, Y.-C. Chang, Wide-angle polarization independent infrared broadband absorbers based on metallic multi-sized disk arrays, *Opt. Express*. 20 (2012) 10376. <https://doi.org/10.1364/OE.20.010376>.
- [32] J. Hendrickson, J. Guo, B. Zhang, W. Buchwald, R. Soref, Wideband perfect light absorber at midwave infrared using multiplexed metal structures, *Opt. Lett.* 37 (2012) 371. <https://doi.org/10.1364/OL.37.000371>.
- [33] B. Zhang, J. Hendrickson, J. Guo, Multispectral near-perfect metamaterial absorbers using spatially multiplexed plasmon resonance metal square structures, *J. Opt. Soc. Am. B*. 30 (2013) 656. <https://doi.org/10.1364/JOSAB.30.000656>.
- [34] Y. Cui, K.H. Fung, J. Xu, H. Ma, Y. Jin, S. He, N.X. Fang, Ultrabroadband Light Absorption by a Sawtooth Anisotropic Metamaterial Slab, *Nano Lett.* 12 (2012) 1443–1447. <https://doi.org/10.1021/nl204118h>.
- [35] N. Zhang, P. Zhou, D. Cheng, X. Weng, J. Xie, L. Deng, Dual-band absorption of mid-infrared metamaterial absorber based on distinct dielectric spacing layers, *Opt. Lett.* 38

- (2013) 1125. <https://doi.org/10.1364/OL.38.001125>.
- [36] Y. Bai, L. Zhao, D. Ju, Y. Jiang, L. Liu, Wide-angle, polarization-independent and dual-band infrared perfect absorber based on L-shaped metamaterial, *Opt. Express*. 23 (2015) 8670. <https://doi.org/10.1364/OE.23.008670>.

APPENDIX 1

Plagiarism report



Page 1 of 42 - Cover Page

Submission ID trn:oid:::27535:99815472

Sushant_dissertation2.docx

 Delhi Technological University

Document Details

Submission ID

trn:oid:::27535:99815472

Submission Date

Jun 8, 2025, 9:16 AM GMT+5:30

Download Date

Jun 8, 2025, 9:22 AM GMT+5:30

File Name

Sushant_dissertation2.docx

File Size

16.6 MB

38 Pages

7,923 Words

42,079 Characters



Page 1 of 42 - Cover Page

Submission ID trn:oid:::27535:99815472

4% Overall Similarity

The combined total of all matches, including overlapping sources, for each database.





Filtered from the Report

- Bibliography
- Small Matches (less than 12 words)




Exclusions

- 7 Excluded Matches

Match Groups

-  **19** Not Cited or Quoted 3%
Matches with neither in-text citation nor quotation marks
-  **1** Missing Quotations 0%
Matches that are still very similar to source material
-  **0** Missing Citation 0%
Matches that have quotation marks, but no in-text citation
-  **0** Cited and Quoted 0%
Matches with in-text citation present, but no quotation marks

Top Sources

- 1%  Internet sources
- 3%  Publications
- 1%  Submitted works (Student Papers)

Integrity Flags

0 Integrity Flags for Review

No suspicious text manipulations found.

Our system's algorithms look deeply at a document for any inconsistencies that would set it apart from a normal submission. If we notice something strange, we flag it for you to review.

A Flag is not necessarily an indicator of a problem. However, we'd recommend you focus your attention there for further review.




Match Groups

- 19** Not Cited or Quoted 3%
Matches with neither in-text citation nor quotation marks
- 1** Missing Quotations 0%
Matches that are still very similar to source material
- 0** Missing Citation 0%
Matches that have quotation marks, but no in-text citation
- 0** Cited and Quoted 0%
Matches with in-text citation present, but no quotation marks

Top Sources

- 1% Internet sources
- 3% Publications
- 1% Submitted works (Student Papers)

Top Sources

The sources with the highest number of matches within the submission. Overlapping sources will not be displayed.

1	Publication	Yan Shi, Xi Ya Xu, Shao Ze Wang, Wen Yue Wei, Quan Wei Wu. "A 1-bit electronical...	<1%
2	Internet	d.docksci.com	<1%
3	Publication	Erdem Aslan, Ekin Aslan, Mustafa Turkmen, Omer Galip Saracoglu. "Metamaterial...	<1%
4	Internet	www.ee.fju.edu.tw	<1%
5	Publication	Nanli Mou, Shulin Sun, Hongxing Dong, Shaohua Dong, Qiong He, Lei Zhou, Long ...	<1%
6	Publication	Yu Liu, Alexis Sebastian. "Effects of external and gap mean flows on sound trans...	<1%
7	Internet	dokumen.pub	<1%
8	Internet	en.wikipedia.org	<1%
9	Publication	Cuilian Xu, Shaobo Qu, Jiafu Wang, Mingbao Yan, Yongqiang Pang, Wenjie Wang, ...	<1%
10	Publication	Dongju Lee, Jung Gyu Hwang, Daechon Lim, Tadayoshi Hara, Sungjoon Lim. "Inci...	<1%

11	Submitted works	Higher Education Commission Pakistan on 2013-07-27	<1%
12	Publication	P. Sinha, T. Mukhopadhyay. "Programmable multi-physical mechanics of mechani...	<1%
13	Publication	Rashidi, A. "Metamaterials Comprising of Plasmonic Nano-spheres and Nanorods:...	<1%
14	Submitted works	Universiti Malaysia Perlis on 2018-11-27	<1%
15	Publication	Yinhui Kan. "Metamaterials for Manipulation of Thermal Radiation and Photolum...	<1%
16	Publication	Zhaofeng Ma, Fei Ding. "Ultra-broadband metamaterial absorber in terahertz reg...	<1%
17	Internet	dergipark.org.tr	<1%